Clim Dyn (2012) 39:3103–3120
DOI 10.1007/s00382-012-1409-x

The Western Mediterranean summer variability and its feedbacks

M. J. OrtizBeviá · F. J. Alvarez-García · A. M. Ruiz de Elvira · G. Liguori · J. H. Carretero

Received: 12 December 2011 / Accepted: 25 May 2012 / Published online: 28 June 2012

Abstract The anomalous climatic variability of the Western Mediterranean in summer, its relationships with the large scale climatic teleconnection modes and its feedbacks from some of these modes are the targets of this study. The most important trait of this variability is the recurrence of warm and cold episodes, that take place at 2–4 year intervals, and which are monitored in the Western Mediterranean Index. We find that the Western Mediterranean events are part of a basin scale mode, and are related to the previous spring atmospheric anomalies. These anomalies are related mainly to the Pacific North America teleconnection pattern and the North Atlantic Oscillation, but also to a number of other climatic modes, connected with the previous two, as the Southern Oscillation, the Indian Core Monsoon and the Scandinavian teleconnection pattern. We identify the main spatial and temporal traits of the Western Mediterranean summer variability, the physical mechanisms at play in the generation of the events and their impacts. Considering the Atlantic Ocean, the Mediterranean events influence the sea surface temperature in the southeastern part of the North Atlantic Gyre. Additionally, they are significantly related to summer precipitation anomalies of the opposite sign in the Baltic basin (Central Germany and Poland) and near the Black Sea. We then estimate the mutual influence that the anomalous previous state of the Western Mediterranean, of the Pacific North America teleconnection pattern and of the North Atlantic Oscillation have on their summer conditions using a simple stochastic model. As the summer Western Mediterranean events have an influence on a part of the Baltic basin, we propose a second stochastic model in order to investigate if thereafter the Baltic basin variability will feedback on the Western Mediterranean sea surface temperature anomalies. Among the variables included in the second model are, in addition to the Western Mediterranean previous state, that of the Baltic Sea and of the Scandinavian teleconnection pattern. From each of the feedback matrices, a linear statistical analysis extracts spatial patterns whose evolution in time exhibits predictive capabilities for the Western Mediterranean evolution in summer and autumn that are above those of persistence, and that could be improved.

Keywords Western Mediterranean summer · Interannual · Feedbacks · Teleconnection indices · North Atlantic Oscillation · Pacific North America · European precipitation · Stochastic models · Baltic · Scandinavia · Predictability

M. J. OrtizBeviá (✉) · F. J. Alvarez-García · A. M. Ruiz de Elvira · G. Liguori · J. H. Carretero
Departamento de Física, Universidad de Alcalá, Alcalá de Henares, 28801 Madrid, Spain
e-mail: ortizbeviamr@gmail.com

1 Introduction

The influence of large scale atmospheric patterns on the Mediterranean climate variability is markedly seasonal. In winter, for instance, the North Atlantic Oscillation (NAO) strongly influences the precipitation (Lamb and Peppler 1987) and also the air temperature variability across the basin (Trigo et al. 2002). This influence also extends to the sea surface temperature and the upper heat content anomalies in the Western Mediterranean (Masina et al. 2004; Tsimplis et al. 2005). In spring and autumn, precipitation and heat content variabilities are modified by the Southern Oscillation (SO) state (van Oldenborgh et al. 2002; Mariotti et al. 2002). Moreover, the Western Mediterranean summer

air temperature anomalies appear to be unrelated to any large scale feature (Lionello et al. 2006).

However, some studies (Millán et al. 2005) have stressed that some coherent warming episodes and the related anomalies observed in summer in the Western Mediterranean region (WM) may be relevant for the atmospheric variability of far away European regions. During these episodes, humidity and contaminants first accumulate in the WM (Gangoiti et al. 2006), and are then exported out of the basin. In some cases, floods in central Europe have been observed to follow these events. In other cases, these episodes lead to a leakage of humid air masses towards northern Africa, which could be related to the anomalous export of Saharan dust through the subtropical Atlantic (Prospero and Lamb 2003). As a consequence, the subtropical North Atlantic boundary layer stability (Lau and Kim 2007; Foltz and McPhaden 2008) could be modified, thereby affecting the number of tropical hurricanes produced during this season. However, Saharan dust export is influenced by the NAO (Moulin et al. 1997). And in the formation of tropical hurricanes, in addition to the atmospheric state, the SST are also relevant, particularly in the Atlantic case (Elsner and Jagger 2006). Tropical hurricane formation is also influenced by the Atlantic Multidecadal Oscillation (AMO), a mode of variability driven by changes in the strength of the Atlantic thermohaline circulation (Zhang and Delworth 2006). These and other possible feedbacks loops are detailed in Figure 11 in Millán (2007). These loops were obtained from theoretical considerations and from empirical mesoscale analysis and forecasting. However, the significance of the highlighted relationships has never been statistically tested and requires of further consideration.

In addition to these mesoscale studies, the ability of the WM to influence the global climate was addressed by Li's (2006) pioneering study. An atmospheric General Circulation Model (GCM) with a relatively coarse resolution, run in perpetual January mode for an extended period, was forced with an anomalous homogeneous cooling of 2 °C in the Mediterranean Sea. The atmospheric response consisted of the development of some baroclinic structure downstream of the cooling along the path of the subtropical jet and of some remote barotropic response. This barotropic response resulted in a deepening of the Aleutian Low and a shallowing of the Icelandic Low. Included among other modeling studies, of relevance to the present research, are a number of experiments that estimate the atmospheric response to North Tropical Atlantic anomalies, performed first with atmospheric GCM (as in Dommenget and Latif 2000), then with coupled GCM (Park and Latif 2005; Wu et al. 2007). Although these models do not include an active Mediterranean sea, the North Atlantic dynamics is able to produce warm and cold Mediterranean events in the air surface temperatures. In particular, Wu et al. (2007) have highlighted the seasonal characteristics of this influence.

Although extremely valuable, all of these studies are very dependent on the model's characteristics and are therefore very dependent on the model's shortcomings. Therefore, for the feedback assessment, we will use statistical techniques on the observational datasets. Stochastic climate models (Hasselmann 1988; Frankignoul and Sennechael 2007) are able to perform the necessary statistical analysis by analysing the covariance matrices between relevant variables with different lags. Additionally, stochastic climate models have important implications for the prediction of climate modes (von Storch et al. 1995; Penland and Magorian 1993; Alexander et al. 2011).

Along these lines, we identify the main traits of the WM summer variability and the large scale signals related to this variability and also the impacts that the variability might have on atmospheric and oceanic anomalies at different spatial scales (global, basin, regional). Moreover we propose a simple stochastic model where the evolution of the WM that leads to the summer variability is explained in terms of the related large scale signals. Another of these models is used to estimate how the summer WMI impacts on the European sector feedbacks on the evolution of the summer WMI. Details of the data and the methodology used for this study are given in Sects. 2 and 3, respectively. The results are described and discussed in Sects. 4 and 5, and the conclusions are presented in Sect. 6.

2 Data

The WM variability will be represented here by the Western Mediterranean Index (WMI) obtained from the ERA-40 SST datafield. The WMI is defined as the average of the summer SST anomalies in the Western Mediterranean region. Further details are given in the Sect. 3.

A set of climatic indices are used to identify the climatic variability at global, basin or regional scale that is significantly related to the WMI. Some of them like the SO Index (Trenberth 1984) and the NAO Index (Jones et al., 1997) are obtained from station data. Other teleconnection indices, such as the Pacific-North America (PNA) Index, the EAWR Index, or the East Atlantic (EA) Index were obtained from gridded fields, according to the procedure of (Barnston and Livezey 1987). Other indices, such as the Sahel Rainfall or the Tropical North Atlantic (TNA) Indices, were obtained as the average of some regional anomalies. A detailed account of the definition and determination of those indices is given in the Table 1. Most of these data are available from the US National Oceanic and Atmospheric Administration [NOAA, at the web site (http://www.esrl.noaa.gov)].

Table 1 Definition of the teleconnection Indices used

Index	Definition
SO	Southern Oscillation Index computed as the Darwin-Tahiti normalized SLP (Trenberth 1984)
NAO	North Atlantic Oscillation Index computed as the Gibraltar-Reykjavik normalized SLP (http://www.cru.uea.ac.uk/~timo/datapages/naoi.htm.)
PNA	Pacific North America teleconnection pattern Index, identified from one of the principal components obtained from an orthogonally rotated analysis (RPCA) of Northern Hemisphere monthly 700 hPa anomalies (Barnston and Livezey 1987).
TNA	Tropical Northern Atlantic Index obtained from averaged anomalies of monthly SST (with respect to the 1951–2000 climatology) in the domain [15°W–57.5°W, 5.5°N–23.5°N] (Enfield et al. 1999)
TSA	Tropical Southern Atlantic Index obtained from averaged anomalies of monthly SST to the region (30W–10E, 0S–20S). It is also called the Gulf of Guinea Index (Enfield et al. 1999)
EAWR	East Atlantic/West Russia teleconnection pattern Index, identified according to Barnston and Livezey (1987) where it is called Eurasia-2 pattern
EA	East Atlantic pattern Index (Barnston and Livezey 1987). The EA is the second most prominent mode of low frequency variability in the North Atlantic, with strong subtropical link
SCAND	Scandinavia pattern Index, computed according to Barnston and Livezey (1987), and known there as Eurasia-1
AMO	The Atlantic Multidecadal Oscillation (AMO) Index, defined as a detrended average of SST anomalies in the North Atlantic (Schlessinger and Ramankutty 1994; Enfield et al. 2001)
TAH	The Tropical Atlantic Hurricane Index was built from monthly totals of Atlantic hurricanes (Landsea et al. 1999)
Sahel	The Sahel Standardized Rainfall Index was computed from averaged precipitation anomalies at 8 stations with almost complete records, in the region (20°N–8°N, 20°W–10°E), according to Janomiak (1988)
DI	Prospero Dust Index (Prospero 2006) consisting of seasonal (JJA) means of monthly observations of African Dust concentrations measured in the Trade Winds at Barbados, for the period 1965–1968 (with two years of missing observations)
CIP	Central Indian Precipitation Index obtained as an average of precipitation anomalies in the Indian Monsoon Core region (18°N–20°N, 73°E–82°E, http://tropmet.res.in)
SWP	Sahel area averaged precipitation Index for Arizona and New Mexico. NCDC, 1994, TD-9640

The Prospero Dust Index (Prospero 2006), consisting of seasonal (JJA) means of monthly observations of African Dust concentrations measured in the Trade Winds at Barbados, for the period 1965-1999 (with two years of missing observations) was obtained from J. Prospero. All of the other indices extend at least from 1958 to 2002. For each of these indices, seasonal time series were segregated, and seasonal indices were built.

Some basic gridded data fields were also used in this study to get further insight of the impacts of the WMI variability and of the related feedbacks. They were obtained from the ERA-40 reanalysis (Uppala et al. 2004), which covers 45 years, from December 1957 to August 2002. From the original monthly data, latitudinally weighted seasonal anomalies were computed (DJF for winter, JJA for summer, and so on). The variables analyzed are the SST, the sea level pressure (SLP), the geopotential height at 500 hPa (Z500) and the zonal and meridional components of the 200 hPa wind (U and V wind respectively). For the purposes of the SST analysis, three regions were selected. The first region is limited to the Western Mediterranean (0.5°W–12°E, 37.5°N–44.5°N) and is represented with a box in Fig. 1a. The second includes the entire Mediterranean Basin (10°W–43°E, 30°N–50°N), the domain of Fig. 2. The third encompasses the Atlantic Ocean north of the tropics (90°W–43°E, 20°N–80°N) (represented in Fig. 6). In the last domain, the SST original resolution (1° × 1°) was regridded to 2° × 2°. The atmospheric fields used in this study cover the Atlantic Ocean region, with the same resolution than the SST field. In some cases north hemispheric atmospheric fields, covering the Northern Hemisphere north of 20°N are used in our analysis. The resolution is then 2.5° × 2.5°.

At some points in our study, timeseries of the WM and also of the Baltic variability that were longer than those provided by the ERA-40 Reanalysis were required. For this purpose, we also included the HadISST1.1 dataset (Rayner et al. 2003), for the period 1870–2002, in our analysis. This dataset consists of monthly observations gridded at 1° × 1° resolution.

The precipitation data were extracted from the global precipitation dataset CRU TS2.1 (Mitchell and Jones 2005).

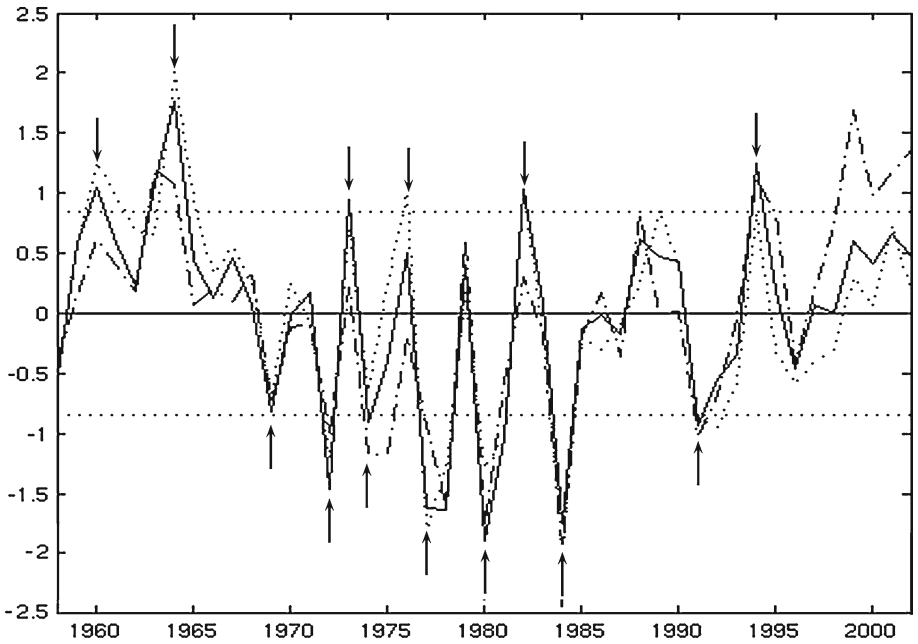

Fig. 1 The first principal component of the WM summer SST anomalies used through this work as Western Mediterranean Index (WMI) (*solid line*). Other versions of the WMI obtained by averaging the SST anomalies (*dotted line*), and the basin scale Index, represented by the 1st PC of the SST anomalies in the whole Mediterranean sea (*dot-dashed line*). Notice how the basin scale Index takes off in the nineties. The straight (*dotted*) lines indicate the thresholds of ±1 standard deviations used to identify the warm/cold events. The warm and cold events identified are pointed at by *arrows*

The data cover the period (1901–2002) at (0.5° × 0.5°) resolution. The domain (12.75°W–41°E, 30.25°N–71.25°N) and the time span (1958–2002) was selected for the purposes of the present study. In connection with the precipitation data, some hydrographic datasets such as the RivDis2.1 dataset (Vorosmarty et al. 1998) were used to further assess the possible impacts of the summer Mediterranean variability. Details of these hydrographic data are presented in Table 2.

3 Methodology

The methodology is tailored for the aims of the present study, to identify the influences in the generation of the WM events and their possible feedbacks outside the Mediterranean area. We use the linear correlation coefficient (r) at different lags between the summer WMI and each of the other indices, to identify the possible relevant interactions. The significance of the correlation (at the chosen 95 % confidence level) is determined by an hypothesis test performed on a Z variable, defined as $Z = 0.5\ln((1+r)/(1-r))$ (Fisher transformation), obtained from the correlation coefficient r. Z is assumed to be asymptotically normally distributed with n-2 degrees of freedom (Fisher 1921).

Once a significant relationship between indices is found, we proceed to analyse the correlation maps of the WMI on the anomalies of the selected variables in the North Atlantic domain. A better understanding of the impact of the events is gained through the use of composites of the same variable for warm and for cold WM events. Warm and cold events are identified as those years where the WMI exceed the ± one standard deviation threshold. Years where the WMI value are inside those limits are considered normal. Compositing is a simple statistical technique that allows for the asymmetries between warm and cold events that are a characteristic of an atmospheric response. Significant features in the composites are identified by two tests: one on the group mean (Terray et al. 2003) and the other on the t values (median and dispersion, Brown and Hall 1999). In these tests, at each grid point, the statistical of the anomalies corresponding to warm (or to cold) years are compared with those of normal years, separately. In this case, the significance is brought down to the 90 % level, to allow for smoother, easier to interpret patterns.

Furthermore, the nature of the interactions between the WM SST and the global atmosphere are investigated with help of a simple statistical model. Let $\mathbf{z}$ represent the instantaneous state of the coupled ocean-atmosphere system. Its evolution is described by the set of prognostic equations

$$\frac{d\mathbf{z}}{dt} = W(\mathbf{z}) \tag{1}$$

where W in general will involve non-linear relationships. The variables included in $\mathbf{z}$ are usually separated in two

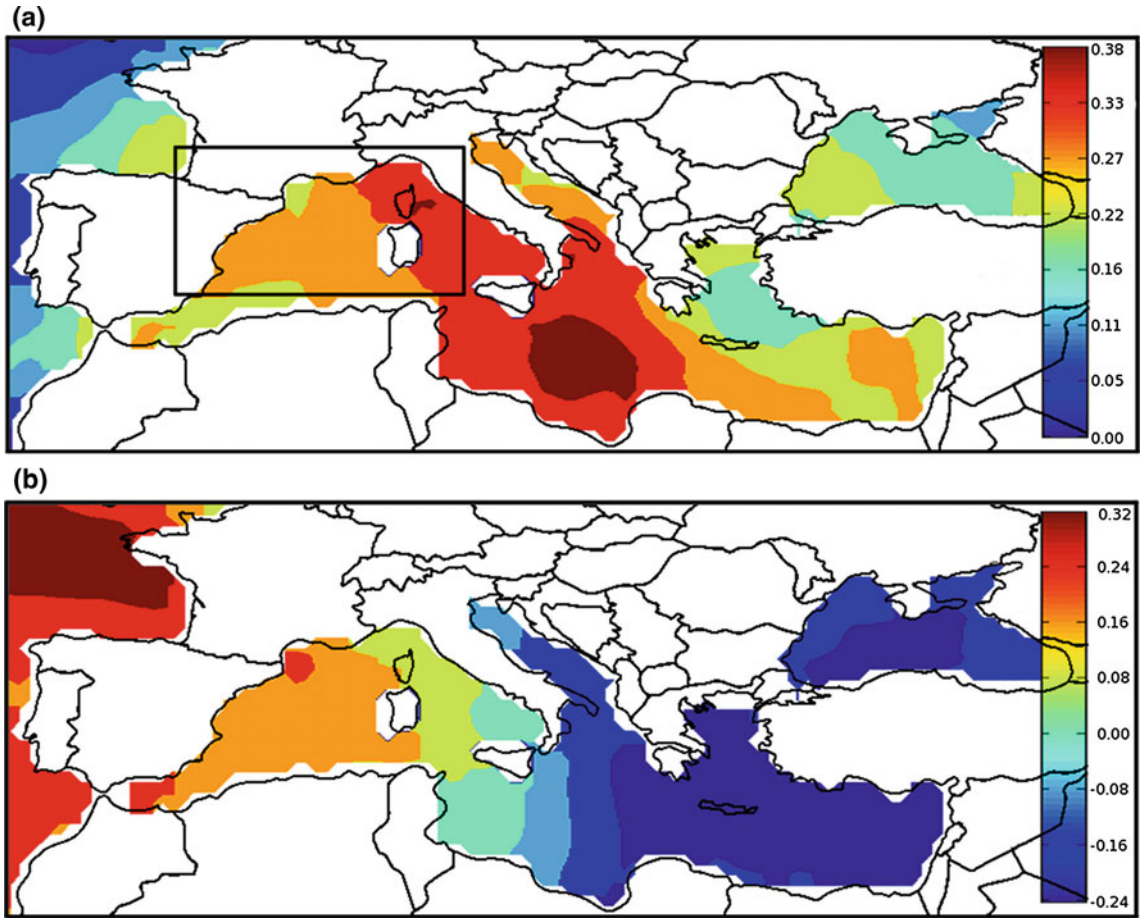

Fig. 2 **a** The first EOF of the ERA-40 SST anomalies, explaining a 45 % of the field variabilty. The *box* encloses the region whose SST anomalies are used to build the WMI. **b** The second EOF of the same field, represented here, explains around a 25 contour interval is 0.2 °C

subsystems (**x**, **y**). The **y** stands for all these variables that represent the evolution of the slowest components of the climate system (i. e. the SST, ice and snow cover anomalies and the part of the atmospheric variability forced by the SST). The **x** represents the fast responding variables, usually identified with the atmospheric weather. The latter variables are represented in stochastic models by a noise term, usually with white characteristics. For small departures from equilibrium, the term W can be linearized, and Eq. (1) reduces to

$$\frac{d\mathbf{y}}{dt} = A\mathbf{y} + w(\mathbf{x}) \tag{2}$$

where A is a matrix (the dynamical or feedbacks matrix) that represents the effects that the present state of the variables has on the future evolution of each of them. This

Table 2 Characterization of the monthly river discharge data

Basin	River	Gauge Station	Coordinates	Period	Average (m^3/s)	Std. Deviation (m^3/s)
Po	Adige	Adige Trento	(11.12E,46.12N)	1925–1979	228	127
				1958–1979	198	92
Po	Po	Piacenza	(09.73E,45.08N)	1925–1979	978	600
				1958–1979	1030	615
Po	Po	Pontelagoscuro	(11.52E,44.93N)	1919–1979	1514	778
				1958–1979	1575	834
Elbe	Elbe	Decin	(14.22E,50.78N)	1870–1984	307	219
				1958–1984	316	200
Danube	Danube	Drobeta-Turnu Severin	(22.44E,44.70N)	1870–1988	5493	2173
				1958–1988	5606	2127

matrix can be identified from the data second moment statistics.

From the eigenvectors of the *A* matrix, a new spatial basis can be determined whose evolution in time is an exponential function of the eigenvalues. Because the *A* matrix is in general non-symmetric, some of the eigenvalues could be complex. Therefore, some of the eigenvectors could represent an oscillatory mode. For this reason, the new basis vectors are usually referred to as the principal oscillation patterns (POP) of the system (Hasselmann 1988). More details about the statistical technique and the POP estimation are given in the "Appendix".

A reduction in the number of degrees of freedom of the system seems necessary in order to obtain results that are easy to interpret. In previous POPs analysis this reduction was carried out by an expansion in the empirical orthogonal functions (EOF) of the system, and further truncation. In the present version the variables that represent the system will be the indices: the WMI, representing the Mediterranean variability, and the other indices that are relevant for its evolution, as reflected in the correlations at different lags represented in Fig. 4.

No filter other than the seasonal mean is used in the present study, except that, in the case of the extended datasets, a band pass filter (Kaylor 1977) was used to help identify the variability corresponding to scales longer than the interannual scales. Additionally, to identify the statistically significant scales, we perform a power spectrum analysis of those time series, smoothing with a 60 years Parzen window, and determine the 95 % confidence interval through the theoretical power spectrum of a fitted AR(1) process.

4 The Western Mediterranean summer variability

4.1 Characterisation of the variability

The WMI used throughout this work to monitor the WM variability is the first principal component (PC) of the SST anomalies at the same season, represented in Fig. 1 with a solid line. This WMI has better statistical properties but is otherwise very similar to the WMI represented with a dotted line; the latter WMI being obtained by averaging the summer SST anomalies over the WM region (0.5°W–12°E, 37.5°N–44.5°N) that is represented inside the box in Fig. 2a. In the same Fig. 1, we depict the first PC of the summer SST anomalies of the entire Mediterranean basin with a dashed line. To make easy the identification and the quasi-periodicities warm and cold events are explicitely pointed with arrows.

The corresponding first EOF, shown in Fig. 2a, explains more than 45 % of the variability of the field. It presents a coherent warming in the entire Mediterranean basin, more important in the western part, and with maximum values towards the centre of the domain (south of the Ionian Sea). The second EOF, represented in Fig. 2b, explains 25 % of the field variance. This last pattern, a dipole with centre of opposite sign in the Western and in the Eastern Mediterranean Sea is sometimes called the Mediterranean Oscillation (Conte et al. 1989).

Warm and cold events, with maximum intensities of roughly ±2 °C and quasi periodicities of around 3-to-5 years are evident in the three curves of Fig. 1a. Additionally, they have been explicitely marked with arrows, for easy identification and also to highlight the quasi-periodicities. There is good agreement between the events

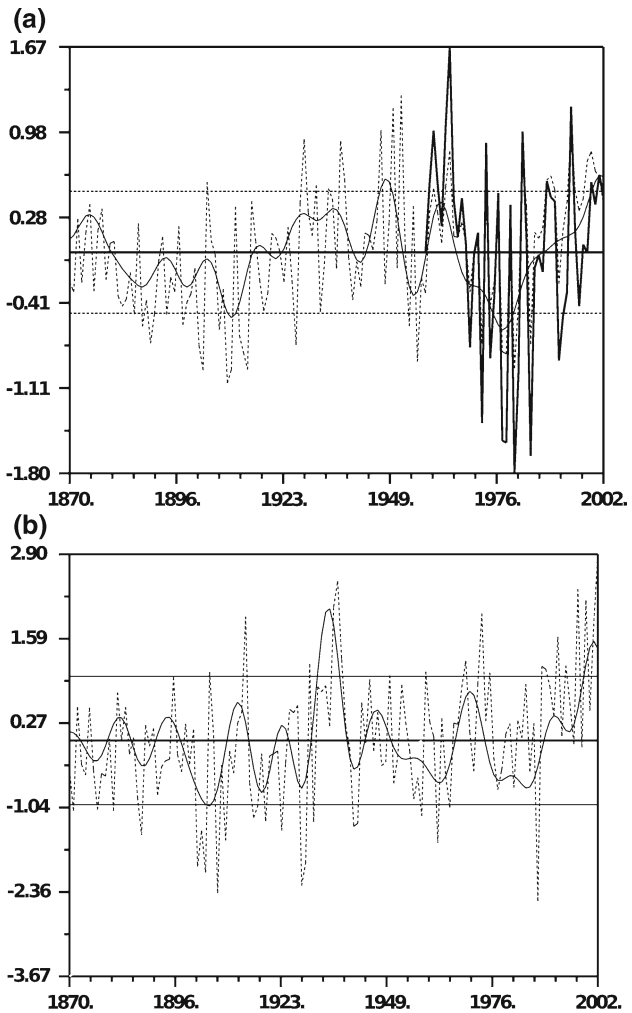

Fig. 3 **a** The extended WMI (*dashed*) against the ERA-40 WMI (*thick solid line*). The low frequency component of the extended WMI is represented with *thick continuous line*. Units are °C. **b** The Baltic Index (*dashed*) and its low frequency component obtained by applying the same band pass filter used for the low frequency extended WMI (*thin continuous line*). Units are °C

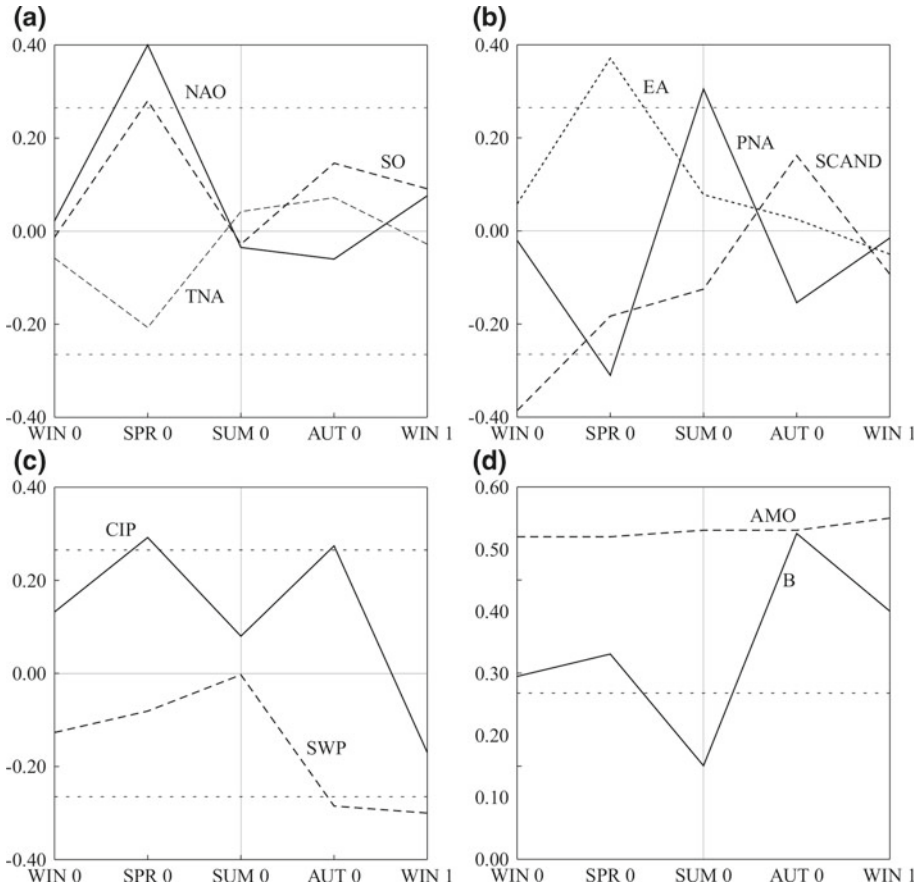

Fig. 4 **a** Correlation between the WMI and the NAO Index (*continuous line*), the SO Index (*long dashed line*) and the North Tropical Atlantic Index (*dashed line*). **b** Correlation between the WMI and the EA teleconnection pattern Index (*dotted line*), the PNA Index (*continuous line*) and the SCAND (Eurasia-1) teleconnection pattern Index (*long dashed line*). **c** Correlation between the WMI and the CIP Index (*solid line*), and the North American SWP Index (*long dashed line*). **d** Correlation between the WMI and the AMO Index (*long dashed line*), and the Baltic Index (*solid line*). The *x* axis goes from the previous winter of the same year (WIN0) to the winter of the following year (WIN1)

identified using the WMI obtained by averaging the SST over the WM region and that yielded by the 1st PC of the WM anomalies, except in the case of the 1976 event. The record include five (six with the 1976 event) warm and seven cold events, some of them extend for more than one year. The warm or cold years are identified using the one standard deviation threshold represented by the straight dotted lines in Fig. 1. Eight out of the 45 years are identified as warm, and nine as cold. The differences in the last part of the record, after 1990, are most visible in the first PC of the SST anomalies for the entire basin.

An extended WMI was built from the HadISST dataset and is represented in Fig. 3a with a short dashed line. The existence of a multidecadal variability in the WMI, which was hinted at in the short Index (represented in this same figure with a thick continuous line), is evident here. Notice in this figure how the warm events appear even during the cold phase of the multidecadal oscillation included in the ERA-40 datasets (years 1967–1990). Moreover it has been found convenient to include in our analysis an extended Baltic Index, defined as the summer (JJA) average of the SST anomalies in the Baltic region and represented in Fig. 3b (also with a short dashed line).

4.2 The relationships with large scale modes

The (summer) WMI is not significantly correlated with either the NAO or the SO Index at the same season. Nevertheless, the WMI correlation with the spring NAO Index and with the spring SO Index are both significant. The latter correlation value shows the importance of atmospheric forcing in the development of the basin scale variability. The correlation of the WMI with the autumn NAO Index and with the autumn SO Index are both negative and not significant.

The behavior of the correlations with lags between -2 (previous winter) to $+2$ (next winter) seasons are depicted in Fig. 4a. Thereafter, we have computed the correlations between the WMI and the EA, SCAND and PNA Indices (depicted in Fig. 4b), the correlations with the CIP and with the SWP Index (represented in Fig. 4c) and the correlation with the AMO and the Baltic Index (shown in Fig. 4d).

For the Scandinavian and the EA Indices, significant correlations with the WMI were found in the preceding winter and spring respectively. In the case of the PNA Index, the spring correlation (negative) and the summer correlation (positive) are significant. Significant positive

values are found in the case of the CIP Index in spring and autumn and in the case of the SWP Index in autumn. The correlation of the WMI with the AMO Index is always significant and the correlation of the WMI with the Baltic Index reaches its maximum in autumn. The correlations between the WMI and some other indices pass the significance test at a lower (90 %) confidence level than in the preceding cases. Such is the case for the (positive) correlation between the Dust Index and the WMI, the (negative) correlation between the Dust Index and the Sahel precipitation Index, and the correlation between the Sahel precipitation Index and the WMI. The correlation between the WMI and the tropical hurricane Index is not significant even at these lower confidence level.

We can then separate the behavior of the teleconnection indices into three groups. Some of the indices, such as the NAO, the SO, the EA and the SCAND, show significant correlations with the WMI at seasons previous to the WM warmings. Those patterns, therefore, influence the generation of the WM events but do not receive a significant back impact. There are other indices like the SWP Index or the Baltic Index where the correlation with the WMI is significant and strongest one season after the events: these are influenced by the WM events. Lastly there are other indices, like the PNA and the CIP Index that show significant correlation before and simultaneously or after the warming events peak. The change of sign observed in the correlation between the PNA Index and the WMI indicates a possible forcing by the Western Mediterranean variability.

4.3 Generation and evolution of the Western Mediterranean events

The significance of the relationships between the WM summer events and some of the teleconnections patterns one or two seasons before, highlights the influence of these patterns in the generation of events. Therefore, the evolution of the WM events will be characterised by the correlation maps of the WMI on the anomalies of relevant variables at the previous winter (antecedent conditions) and spring (onset), the summer (warm events) and the autumn afterwards (decay).

1. The antecedent conditions (that is, regions with statistical significance in the correlation maps) can be found no earlier than the previous winter and only in the precipitation anomalies (correlation CIP Index-WMI, Fig. 4c), the SLP and the 200 hPa U and V anomalous fields. Composites of the last fields for the winters preceding warm events and for the cold events are represented respectively in the left and right column of Fig. 5. The main significant features in the warm composites are to be found in the subtropical Pacific (SLP and U-wind fields, Fig. 5b, d) and near the North Pole and over the East Central Asia and Mongolia (V-wind field, Fig. 5f). The areas of significance are larger for the cold event composites, and correspond to the subtropical Pacific (U-wind), the North Pacific (SLP and V-wind), New Foundland (V-wind and U-wind), East Central Asia (SLP and V-wind) and the strip going from Scandinavia to the Eastern Mediterranean (V-wind). Orographically or diabatically forced Rossby waves (Hoskins and Karoly 1981; Orlanski and Solman 2010) are evident in the winter V-wind composite for cold events. No significant features are to be found either in the regression map of the WMI on the winter SST anomalies or in the corresponding composites.
2. The onset of the WM events occurs in spring and is represented in the Fig. 6a, b. The WMI regression on the SST anomalies (Fig. 6a) presents positive significant values in the WM region that extend along the coast of Portugal and can be related to anomalous winds of opposite sign along the coast of Iberia. They also show significant wave activity along the Gulf Stream path. The main feature of the SLP regression map (Fig. 6b), is a region of negative correlations near the British Islands. This pattern is a synoptic feature that corresponds to transitions between two large scale atmospheric regimes, Zonal to Greenland Anticyclone (SánchezGómez and Terray 2005) and that is associated to intense precipitation events in Western France. However, this trait is statistically significant only in the cold event composites. For cold events the Icelandic Low and consequently the NAO index are weakened. For warm events, the Northern Hemisphere correlation maps (not shown) reveals anomalous significant high pressures in the Aleutian Low (negative phase of PNA) while conditions in the North Atlantic are similar to those of the positive phase of the EA teleconnection pattern.
3. The WM events take place in summer. In the case of the warm events, the anomalous low pressures in the Alboran Sea make the NAO Index drop to negligible values. On the contrary the PNA index shifts towards small positive values. This is consistent with the propagation of barotropic structures from the eastern Mediterranean to the North Pacific, as was observed in Li's (2006) experiment. A significant ridge of high pressure appears in central Europe (Germany, Poland, Ukraine) (Fig. 6c). The warming in the Western Atlantic is now South of the Bermudas (Fig. 6d), while in the SLP field there are significant positive SLP anomalies over the Lakes Region, connected with SST anomalies of the same sign in the Bermuda High region.

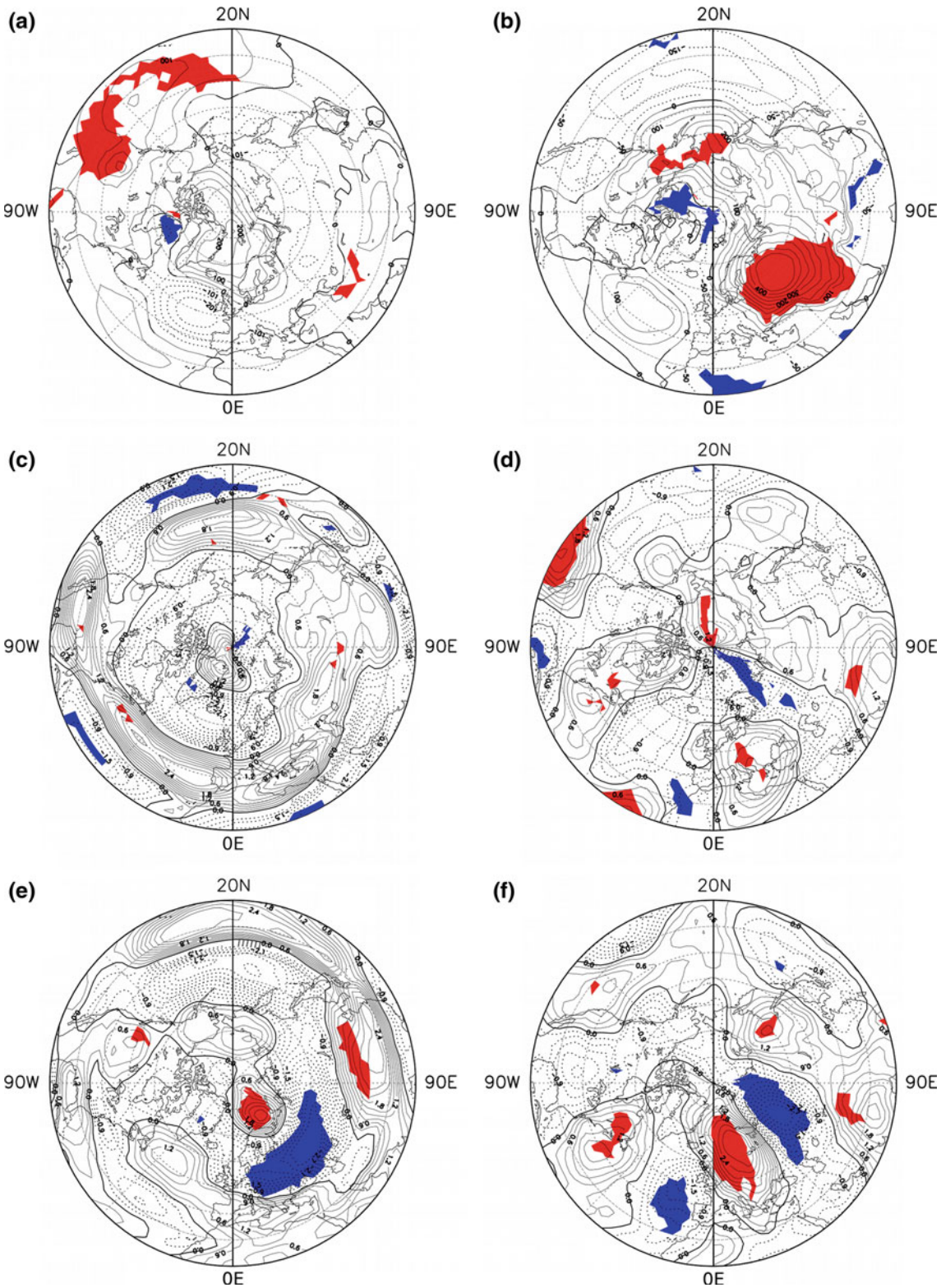

Fig. 5 Antecedent conditions in the winter previous to warm events: composites of **a** SLP anomalies, **c** Zonal U-wind, **e** Meridional V-wind anomalies. Antecedent conditions in the winter previous to cold events: composites of **b** SLP anomalies. **d** U-wind anomalies, **f** V-wind anomalies. Regions where the composites are found significant at the 90 % confidence level by a statistical test are *shaded red* (positive) or *blue* (negative). Contour interval is 50 hPa for SLP composites and 0.3 m/s for the winds

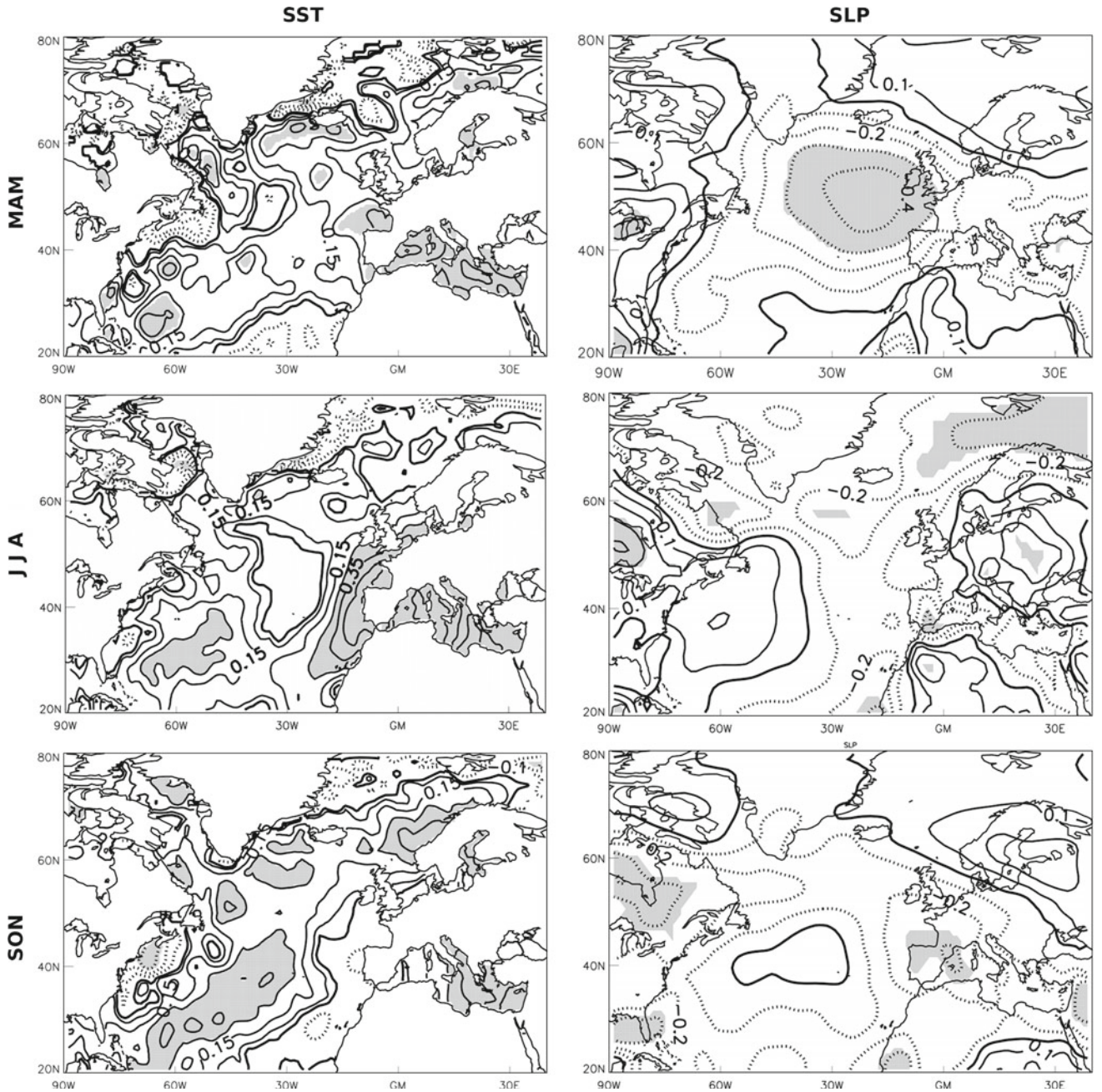

Fig. 6 Correlation maps between the WMI and: **a** the spring North Atlantic SST anomalies, **b** the spring North Atlantic SLP anomalies, **c** the summer North Atlantic SST anomalies, **d** the summer North Atlantic SLP anomalies, **e** the autumn North Atlantic SST anomalies and **f** the autumn North Atlantic SLP anomalies. Regions where the correlations are found significant at the 95 % confidence level by a statistical test are shaded. Contour interval is 0.1

The SST anomalies of the same sign than the events to be found along the Iberian and North African coasts (Fig. 6d) can be explained by the anomalous upwelling along these coasts, induced by the significant SLP anomalies in the Gibraltar region. The influence of the WMI on the SST anomalies near the Bermudas can be explained by the propagation of Rossby waves induced by the SST east Atlantic anomalies, that will continue along the Gulf Stream. However SST anomalies in the Bermuda region are statistically significant only in the warm event composites. Additionally, they are also influenced by the PNA teleconnection pattern and by tropical forcings.

The composites of the precipitation anomalies for warm and cold events are depicted in Fig. 7. The warm composite, represented in Fig. 7a, associates the WM

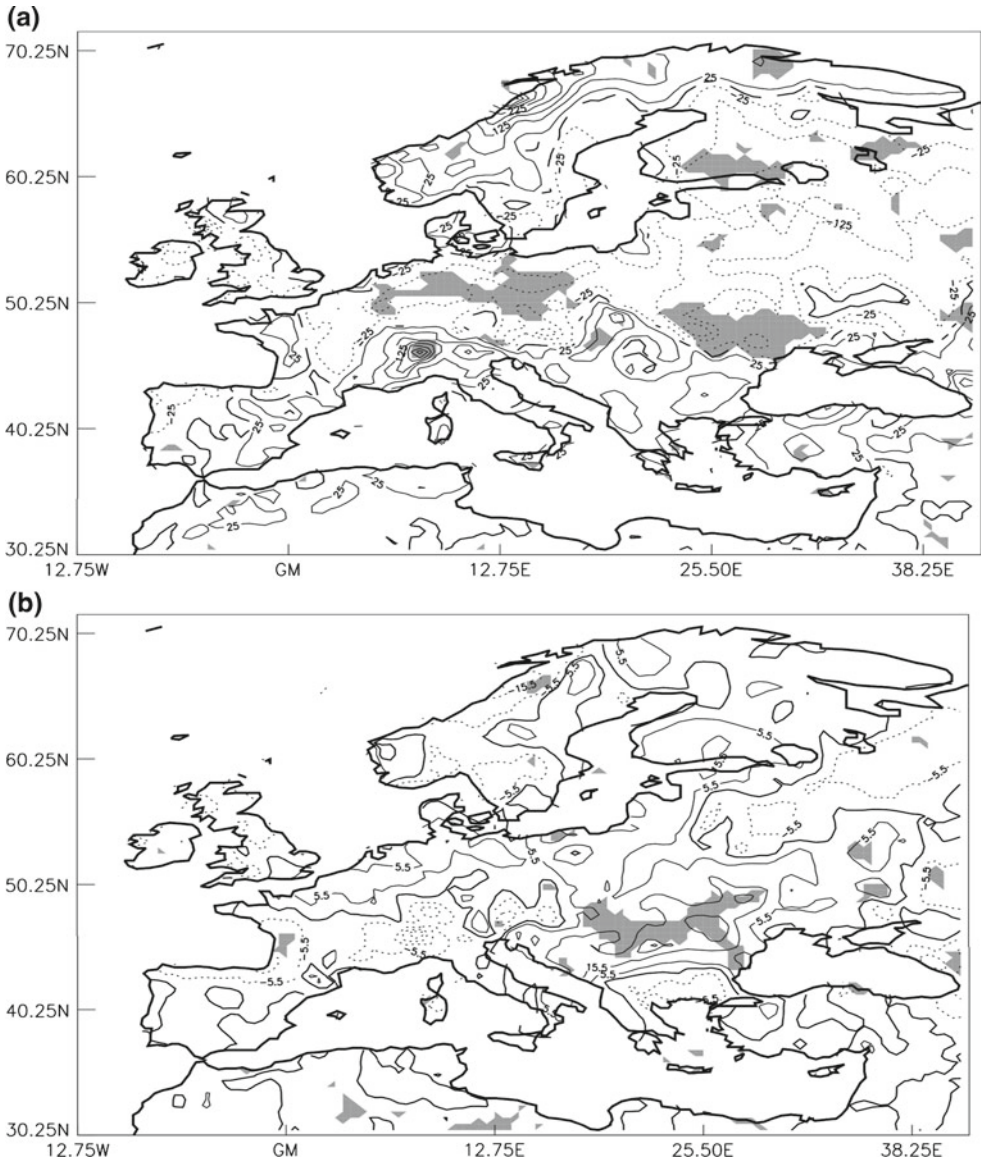

Fig. 7 **a** Composites of precipitation anomalies in the extended Mediterranean domain during warm events. Contour interval is 25 mm. **b** Composites during cold events. Regions shaded were found significant at the 90 % confidence. Contour interval is 5 mm

events with positive precipitation anomalies in a reduced region of the Italian Alps, and with negative precipitation anomalies in parts of Germany, Poland and the Ukraine and the northern shore of the Botnia Gulf. The cold composite, shown in Fig. 7b, presents significant positive precipitation anomalies along the low course of the Danube. The contribution of the WM events to the precipitation anomalies in the region can be explained by the basin induced wind anomalies in the region. Although in summer, as in winter, the mean wind circulation in the Mediterranean region is to the south, there are some stretches of southerly flows across or bordering the Dolomites that will bring additional moisture to the south of Germany and Poland, and to the Danube Valley (Kallos et al. 2007). During extreme Mediterranean events, these southerly flows (and therefore the moisture transport to the north) will be weakened/enhanced, depending on the phase of the events. This could explain the enhancement of the incipient negative anomalies produced by the anomalous spring warming in those regions.

4. Decay conditions appear in autumn, as the anomalous SST are displaced to the eastern Mediterranean Sea (Fig. 6f). The SST anomalies near Bermuda now reaches the Central Atlantic and there are signs of wavelike propagation along the Gulf Stream (Fig. 6e). The ridge of high pressure in the Baltic is now centred in the Gulf of Finland.

Additionaly, in the case of the discharge data, seasonal averages with two different definitions (DJF, MAM in one case and JFM, AMJ in the other) have been used to achieve

a better characterization of the impact of the WMI. The correlations between the (JJA) WMI and the anomalies at three discharge stations at two Italian rivers (Po and Adige) are represented in Fig. 8a. In this case, the WM events were preceded the previous spring by significant negative anomalies, that, in two of the cases, increased in JJA (the months when the WMI was computed). Thereafter, the correlation between the autumn discharge anomalies and the WMI is positive and statistically significant. In Fig. 8b we have represented the correlations in the case of two long European rivers (the Elbe and the Danube). These results are in good agreement with the warm composites of Fig. 7. In the case of the Elbe and the Danube rivers, the warm events were followed by negative precipitation anomalies.

The lower values of the correlation between the WMI and the Dust Index are due in part to the reduced length of the Dust observations, but also to the influence of other factors, like the change of sign of the AMO during the eighties. Nevertheless, we have found that during cold events the export of Dust is considerably reduced and the same applies to the number of hurricanes in the bimonth June–July.

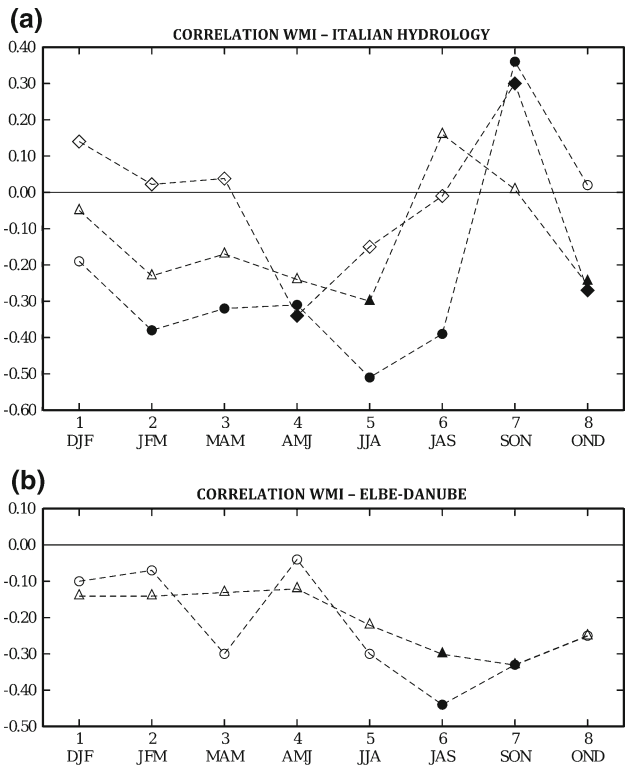

Fig. 8 Correlations between the WMI index and several river discharge data. **a** Anomalies computed at stations south of the Italian Alps (Boara Pisani at Adige (*rombs*), Pontelagoscuro (*triangles*) and Piacenza (*circles*) at Po. **b** Anomalies computed from data of the station Drobeta (*triangles*) at the Danube and the station Decin (*circles*) at the Elbe. Statistically significant (at the 95 % confidence level) correlations are represented with *filled symbols*

5 Stochastic models and feedbacks matrices for the Western Mediterranean variability

The simplest stochastic model for the summer WMI variability should include the effect of the initial conditions (spring WMI) and the effect of the atmospheric signals that are best correlated with the summer WMI: the spring NAO index (highest correlation) and the spring PNA (significant correlations at the two seasons involved, spring and summer). The other atmospheric signals with significant correlation are also either highly correlated with the spring NAO (such as the winter SCAND or the spring EA), highly correlated with the spring PNA, or their correlation with the summer WMI are barely significant (CIP). Let $\mathbf{y}_{m,i}$ represent the state of one of the indices m at time i. The m subindex will take the value 1 for the WMI, 2 for the PNA Index and 3 for the NAO Index. The evolution of the Western Mediterranean coupled atmosphere-ocean system will be represented by the stochastic equation

$$y_{m,i+1} - y_{m,i} = \Delta t \left(\sum_{k=1}^{3} a_{m,k} y_{k,i} + w_m(t) \right) \tag{3}$$

where the $w_m(t)$ is a white noise term, that accounts for all of the rest of the atmospheric effects that have not been considered. The $a_{m,k}$ were determined according to the procedure detailed in the Sect. 3. The values obtained for the feedback matrix A are

$$A = \begin{pmatrix} -0.55 & -0.56 \times 10^{-3} {}^{\circ}C/m^2 s^{-2} & 0.022\ {}^{\circ}C/hPa \\ 44.72\ m^2 s^{-2}/{}^{\circ}C & -0.46 & 4.0\ m^2 s^{-2}/hPa \\ 1.03\ hPa/{}^{\circ}C & -0.19 \times 10^{-3}\ hPa/m^2 s^{-2} & -1. \end{pmatrix}$$

From the analysis of the coefficients of the A matrix, we see that the previous spring state (coefficients on the diagonal + 1) is important only in the case of the WMI (first row) and the PNA Index. In the NAO case (third row), the only important feedback appears to be the oceanic feedback.

From the dynamical A matrix, the POP, the POP eigenvalues and POP time coefficients were identified. Two of the eigenvalues are complex conjugated, pointing to an oscillatory pair of modes, with a period of 2.1 years, and 3 years of e-folding time. As the correlation between the time coefficients of the POP 1/2 was originally too high (roughly 0.8), they have been rotated to ensure more orthogonality (Fig. 9). As a result, the correlation value of the summer WMI with the POP 1 time coefficient (0.6) is higher than its correlation value (0.5) with the spring WMI (persistence). The correlation between the POP 2 and the POP 3 is sizeable. The time coefficients of the pair 1/2 are represented in Fig. 10a. The trend is well captured as are the propagating features (the time coefficient of POP1

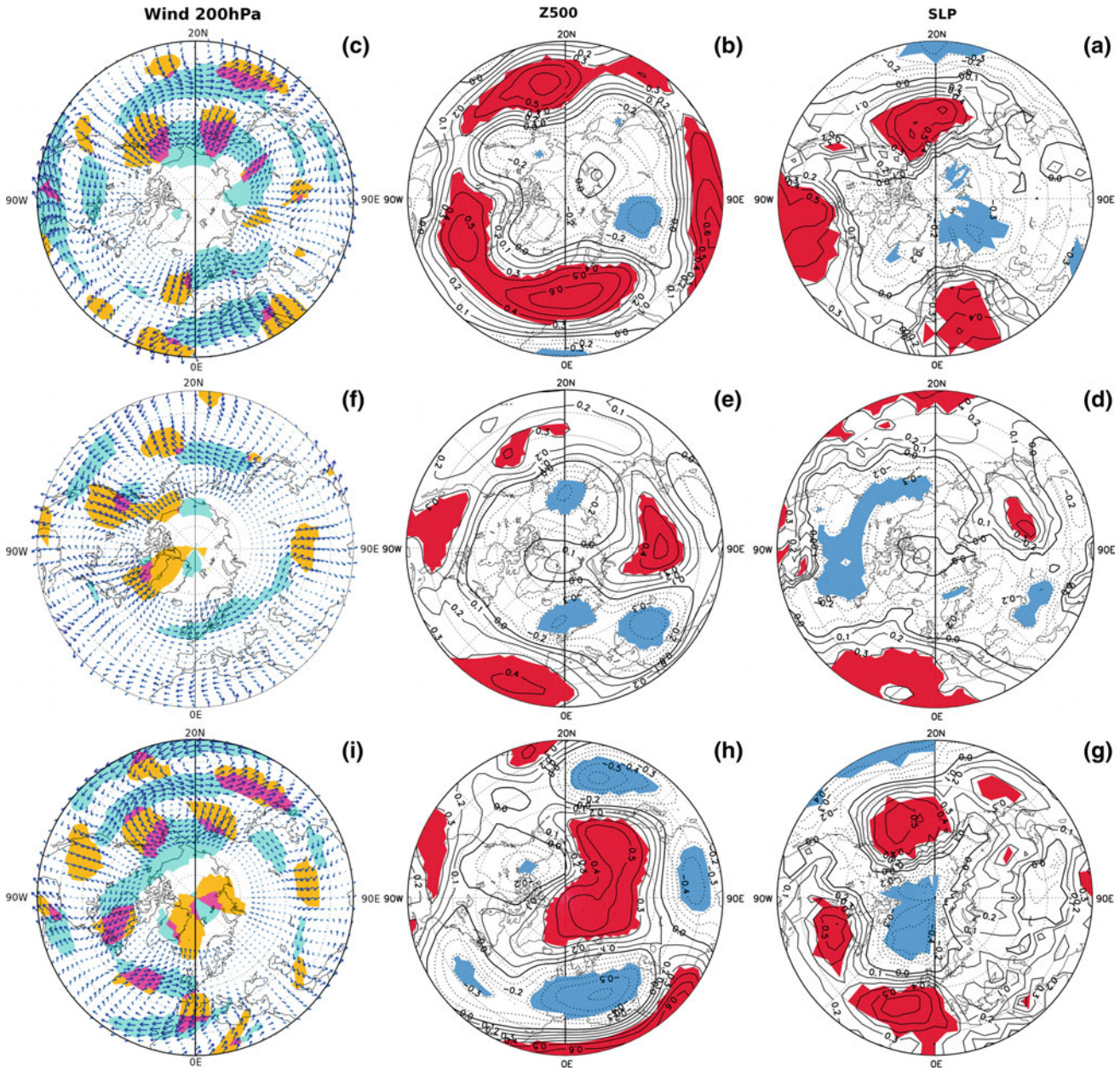

Fig. 9 *Top row* Patterns associated to the POP 1 of the pair 1/2 in the spring anomalous fields of **a** SLP. **b** Z500 and **c** 200 hPa winds associated to the spring-to-summer feedbacks. *Middle row* Patterns associated to the POP 2 of the pair 1/2 in anomalous fields of **d** SLP, **e** Z500, **f** 200 hPa winds the previous winter. *Bottom row* patterns associated to the POP 3 in the spring anomalous field of **g** SLP, **h** Z500 hPa, **i** 200 hPa winds. For the SLP and Z500 patterns regions found statistically significant at the 95 % confidence level are *shaded* (*red* for positive correlations, *blue* for negative ones). In the case of the 200 hPa wind, the statistical significant regions are *shaded yellow* in the case of the U-wind associated pattern, *blue* in that of the V-wind, *magenta* for significance in both fields. Contour interval is 0.1

precedes that of POP2 specially in the last part of the record).

The associated patterns, obtained as the correlation maps of the POP time coefficients with the anomalous fields of the SLP, the Z500 and the 200 hPa wind at spring (POP 1 and 3) or at the previous winter (POP 2), are represented in Fig. 9. The POP 1 is associated to a north-south SLP gradient in the European sector (Fig. 9a), an enhanced planetary wave activity in the Z500 hPa anomalous field (Fig. 9b) and significant anomalies in the 200 hPa wind field that are consistent with those associated to the PNA pattern. Moreover, the POP 1 associated pattern in the

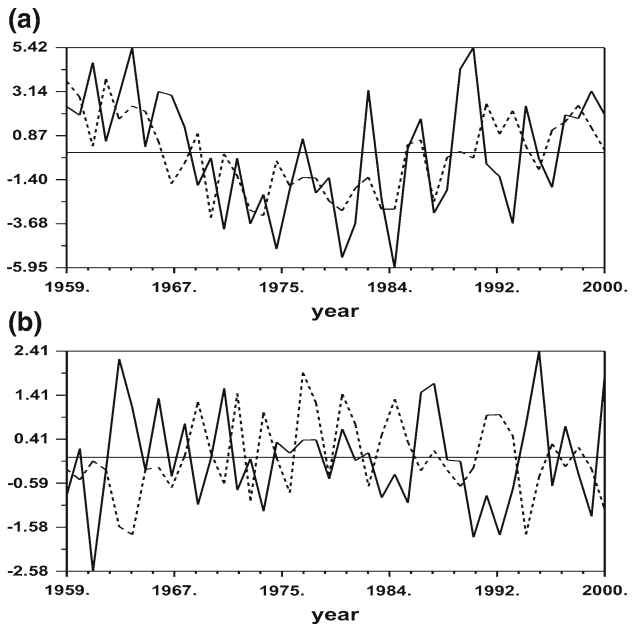

Fig. 10 Time coefficients of the POP 1 (represented with *solid line*) and of the POP 2 (with *dashed line*) of the pair 1/2 determined for **a** summer, **b** autumn

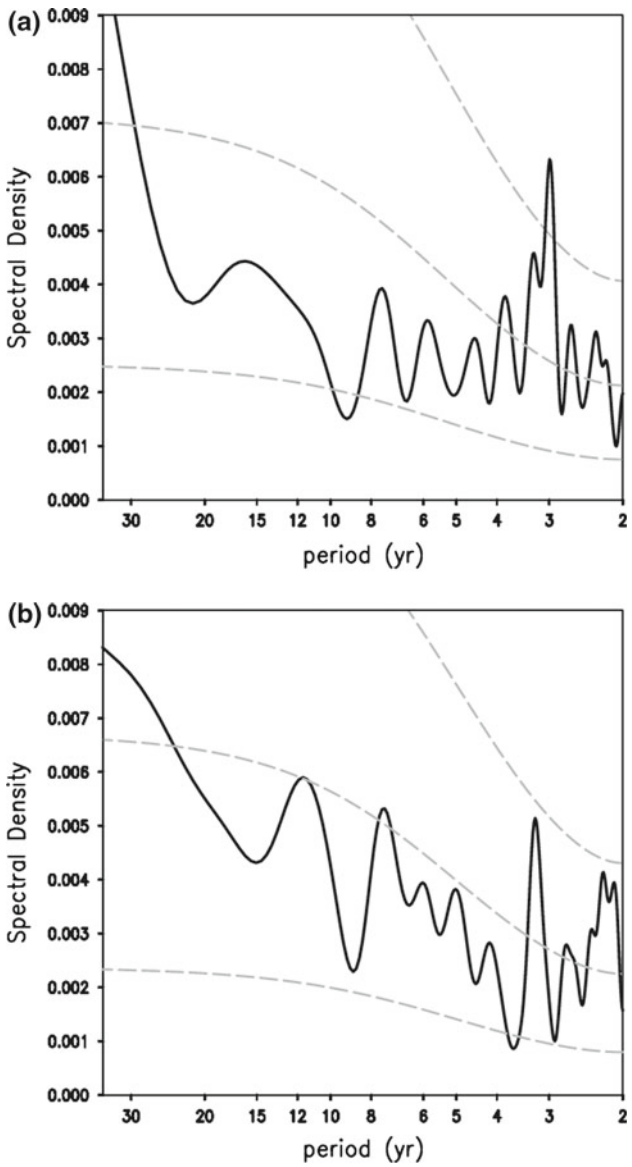

Fig. 11 **a** Power spectrum of the extended Western Mediterranean Index computed using a 60-year Parzen window (*solid*) and theoretical power spectrum of fitted AR(1) process, and the 95 % confidence interval (*dashed*). **b** Power spectrum of the Baltic Index, computed as an average of summer (JJA) anomalies in the Baltic region. Spectral window details and confidence intervals as in **a**

U-wind field presents for warm WM events negative anomalies in the southern part of the U.S. and positive ones near Canada, that are consistent with an anomalous northward displacement of the polar jet, and a similar feature is present in the European sector. While the POP 1 represents the part of the spring variability related to the summer WM state, the POP 2 accounts for the related conditions at a previous season. Therefore the patterns associated in winter to the POP 2 are represented in Fig. 9d–f and show significant SLP and Z500 anomalies of the same sign in the subtropics, and significant anomalies of opposite sign in both fields at northern latitudes. The SLP dipole Kazhastan-Mongolia in the SLP field can be connected with the V-wind anomalies that modify the path of the subtropical jet. The pattern associated to the POP 3 in the Mediterranean region presents a change of signs from spring (negative) to summer (positive).

The connection between the WM variability and the Baltic variability in summer is assessed from the spectral characteristics of both indices, shown in Fig. 11a, b respectively. There is a peak in the WMI spectrum, corresponding to a 3 year period that is statistically significant, and another peak at the same period in the Baltic Index spectrum is almost significant at the chosen (95 %) confidence value. Given the impact that the WM events have in the Baltic basin, as shown in Fig. 7 (in particular the negative precipitation anomalies in the southern part of the basin), it could be that the basin in turn influences the WM. The link is further supported by the value of the correlation between the WMI and the Baltic Index in autumn (Fig. 4d). We search to establish whether this connection comes from a common forcing by the North Atlantic or from the atmospheric anomalies forced by the Mediterranean variability. To address this point, we have applied the same feedback statistical model to the evolution of the system from its summer conditions. In the model equation, the m subindex will take the value 1 for the Baltic Index, 2 for the SCAND Index and 3 in the case of the WMI, and the subindex i stand for summer. The estimated values of the coefficients of the autumn feedback matrix in this case are:

$$A = \begin{pmatrix} -0.8 & -0.8 \times 10^{-4}\ ^{\circ}C/m^2s^{-2} & 0.15 \\ -18.8\ m^2s^{-2}/^{\circ}C & -0.85 & 59.82\ m^2s^{-2}/^{\circ}C \\ 0.125 & -0.23 \times 10^{-2}\ ^{\circ}C/m^2s^{-2} & -0.65 \end{pmatrix}$$

According to the coefficients of the A matrix, the evolution of the Baltic Index is dominated by the negative feedbacks of the Baltic and SCAND variability (the WMI has a positive coefficient). In the evolution of the SCAND Index, only the SCAND Index and the WMI contribute more. For the evolution of the autumn WMI, the three indices seem important.

As in the preceding case, the POP, eigenvalues and temporal coefficients were determined from the feedbacks A matrix. Also in this case, two of the eigenvalues are complex conjugated, pointing to an oscillatory pair of modes, with a period of 2.2 years, and 8.6 years of e-folding time. The third eigenvalue is real (e-folding time of 1.3 years). The correlation between the time coefficients of POP 1/2, although significant, is not too high. The correlations between the autumn Baltic Index and the time coefficients of the pair 1/2 are sizeable in the first case and negligible in the last case (0.41/0.01 respectively), that with the POP 3 time coefficient are statistically significant (0.33). Time coefficients of the pair 1/2 are represented in Fig. 10b. Propagation characteristics are in this case less evident than in the case of the summer conditions.

The correlations of the autumn WM Index with the time coefficients of the POP pair 1/2 are significant (0.29/ 0.32 respectively). The autumn WM Index is not significantly correlated with the POP 3 time coefficient (0.12), however the value of the correlation between this WMI with the time series obtained by adding the time coefficients of POP1 and POP3 is important (0.6). The correlation values of the Baltic Index and the WM Index in autumn with their previous values (skill of persistence) are 0.39 and 0.43 respectively, considerably lower. Therefore the potential for predictability of the Baltic and WM Indices of the two time series supplied by the stochastic model is above those of persistence, and in the last case (the autumn WMI), could be improved to become very useful.

6 Conclusions

The present study uses statistical analysis to investigate the WM variability in summer, its dependence on global and regional climatic signals, and its (possible) feedbacks on these signals. The main features of the WM variability are the quasi periodical warm and cold events, with an amplitude of approximately ±2 °C. These events are related to a mode of variability of the entire basin, that consists of an uniform pattern of the same sign and is well represented by the first EOF of the summer SST anomalies in the western Mediterranean. The corresponding first PC is used here as an index to identify the events and the years (warm and cold) that exceed the one standard deviation threshold. In our sample, that corresponds to the time span covered by the ERA-40 Reanalysis, cold events are relatively better sampled. This could be explained by the phase of the multidecadal variability that appears superimposed to those of the WM events. However, warm events continue to take place even in that conditions, although they are least frequent.

Then we consider the mutual influences between the WM events and some global and regional signals, each of them characterised by an Index, as defined in Table 1. Some other indices, like the Atlantic Dust Index, the Atlantic Hurricane Index or the Baltic Index are used to investigate the possible impacts of the WM events. In a first step, we use the correlation between one of those indices and the WMI to detect possible influences. Our analysis highlights a special relationship between the WM summer variability and the PNA: significant correlation before and during the events, while other indices present significant correlation only before or after the events. The independence of the anomalous variability of the WM basin in summer with respect to the simultaneous Atlantic variability is supported by the lack of correlation between the WMI and the summer NAO Index, and by the lack of statistical significance near the NAO centres of action in the correlation maps between the WMI and the SST anomalies. The sizeable correlation value between the WMI and the previous spring NAO Index indicates that the previous NAO state is important for the generation of the WM events. The influence of the spring SO Index is barely significant, and a part of that influence is conveyed through the NAO and through the PNA signals. Most of these relationships have been reported in the literature, but were never explored and presented in this systematic way.

With respect to the generation of the events, the analysis of the correlation maps of Fig. 6 shows significant SST anomalies in the WM region in the spring previous to the events. The sign of these spring anomalies, in agreement with that of the WM events, tends to be in opposition to the PNA phase. The important part that two aspects of the Artic Oscillation, the PNA and the NAO have in the generation of the events is highlighted by both, the composite maps (Fig. 5) and the correlation maps (Fig. 6). The propagation of planetary waves from the North Pacific two seasons ahead seems to be a relevant physical mechanism for this influence (supported by the composites of Fig. 5 and by the associated patterns obtained from the feedback model in Fig. 9). In addition, the importance of SLP anomalies over Africa in the generation of the events (not significant in the correlation maps) is significant in the associated patterns to

the POP 2 in the feedback model. Considering the North Atlantic influence in spring, a pattern of anomalous high pressures south of Greenland is shown to be relevant for the generation of the cold events by composites, correlation maps and associated patterns alike. Moreover, the events tend to be preceded by spring precipitation anomalies of opposite sign, a trait supported by the correlation maps of the WMI on the spring precipitation anomalies (not shown) and by the values of the correlations between the WMI and the spring river discharge data (Fig. 8).

Concerning the impacts of the WM events on the North Atlantic region in summer, the only traits whose attribution seems clear are the SLP anomalies of the opposite signs in the Alboran sea, and the related SST anomalies along the coasts of Iberia and North Africa. In other significant traits of the SST and SLP composites, like the warming near the Bermuda High and its propagation, it is hard to separate the WM influence from those of the other PNA related signals. There is another signal in the European sector that can be connected to the WM events: the precipitation anomalies of the same sign in a reduced region of northern Italy and of opposite sign in central Europe and near the Black Sea, supported by the composites of Fig. 7 and the correlations between the WMI and the discharge anomalies of some rivers that are relevant for our study (Fig. 8). We do not have notice of these features been highlighted before. Contrarily, the correlations with the Atlantic Dust Index in summer and with the Tropical Hurricane Index in June–July can be explained by the effects of the spring anomalies of precipitation and temperature in the North African regions. A rainy and cold spring would favour less dust export and less tropical hurricane formation. The first of these results was hinted at in Moulin et al. (1997), the second is, to our knowledge, novel.

Furthermore, through the use of an stochastic model, we can assess not only the influence of the PNA and NAO signals on the WM events, but also the influence that these events might have on the global signals. With respect to the first issue, the estimated values of the feedbacks matrices shows that the influence is important enough and can be used to provide patterns with a predictive potential for the WMI. Concerning the second question, the corresponding coefficients in the feedbacks matrices indicate that although the influence of the WM events on the NAO and on the PNA exists (the coefficients are statistically significant), their values are not enough to provide any potential for predictability.

Lastly, we assess the feedbacks that the variability of regions significantly influenced by the WM events might exert in turn on the evolution of the WM anomalies (one season ahead). Here again the use of another linear stochastic model allows for the determination of those feedbacks. In this case, the variables are the WMI, the Baltic Index and the Scandinavian teleconnection pattern Index. As in the preceding case, the feedbacks matrices is able to supply with predictors whose hindcast skills for the autumn Baltic and WM Indices are above those produced by assuming persistence and, in the case of the WM, that might be useful. To our knowledge these relationships were never considered in this way before.

Although the stochastic models have already been used to represent climatic variability, the formulation in terms of teleconnection indices that we propose here to determine the feedbacks between regional and basin scale variability is quite innovative. Additionally, to our knowledge, the Western Mediterranean variability has never before being represented by such models. As shown in a series of paper by Penland, starting with Penland and Magorian (1993), the full predictive capabilities of the stochastic models are enhanced when the stochastic equation forced with noise is solved. This set up, that in the case of the summer WMI would fully incorporate the predictive capabilities of the first and third POP together is currently being explored.

Acknowledgments Thanks are due to M. Millán (CEAM), for suggesting this topic. This work was financially supported by the CIRCE EU project (GOCE-036961). CIRCE coordinator, Antonio Navarra, is heartely thanked. The Spanish Meteorological Agency (AEMET) is acknowledged for providing access to the ERA-40 data sets. The USA National Oceanic and Atmospheric Administration (NOAA) must also be acknowledged here for the preparation of some of the climatic indices used in this work. The three anonymous reviewers of this paper are thanked here for comments.

Appendix

The principal oscillation pattern (POP) analysis

Let a system be described by a state vector ($\mathbf{z} = \{z_j,\ j = 1, n\}$) where the z_j represent the centered values of one or several variables. Let ($\mathbf{z}_i,\ i = 1, m$) represent m samples of the state vector $\mathbf{z}$, obtained at m different times. Let the time evolution of the system be represented by a linear stochastic model

$$\frac{d\mathbf{z}_j}{dt} = A\mathbf{z} + \mathbf{n} \tag{4}$$

where A is the dynamical or feedback matrix that represents the response of the system to changes produced by the forcing, and $\mathbf{n}$ represents the 'noise', that we assume to be stationary, gaussian and delta correlated.

The finite difference equivalent of Eq. (4) is

$$\frac{\mathbf{z}_{i+1} - \mathbf{z}_i}{\Delta t} = A\mathbf{z}_i + \mathbf{n}_i \tag{5}$$

with $\Delta t = 1$. From this equation the dynamical matrix can be determined as

$$A = \frac{<\mathbf{z}_{i+1}\mathbf{z}_i> - <\mathbf{z}_i\mathbf{z}_i>}{<\mathbf{z}_i\mathbf{z}_i>} \tag{6}$$

where the angular brackets denote averages to m samples. This can be written in terms of C_1 and C_0, covariance matrices at lag 1 and 0, respectively, as:

$$A = \frac{C_1 - C_0}{C_0} \tag{7}$$

In this way, we take out of the feedbacks coefficients the part of the cross-covariance between each pair of variables that is determined by their own autocovariances, and that introduced by the common cross-covariance that they have with a third variable. Solutions to the deterministic part of Eq. (5) can be written as

$$\mathbf{z}_i = \sum_{k=1}^{n} C_k e^{\mu_k \Delta t_i} \mathbf{u}_k; \quad \Delta t_i = t_i - t_0, i = 1, k \tag{8}$$

where the characteristic exponents μ_k can be obtained from the eigenvalues λ_k of the dynamical matrix A, $\mu_k = \ln(\lambda_k)$, and the $\mathbf{u}_k$ are the corresponding eigenvectors.

As the dynamical matrix A is non-symmetric, its eigenvectors and eigenvalues will be in general complex. Also, due to the assumption of stationarity, the absolute values $|\lambda_k|$ are lower than 1, and therefore the exponents μ_k are negative. The oscillations are always damped. If the number of complex eigenvalues is l_i, Eq. (8) can be written as

$$z_i = \sum_{k=1}^{l_i} c_k e^{\mu_k \Delta t_i} [\mathrm{Re}(\mathbf{u}_k) + \imath\, \mathrm{Im}(\mathbf{u}_k)] + \sum_{l_i+1}^{n} c_k e^{\mu_k \Delta t_i} \mathbf{u}_k. \tag{9}$$

If we denote $\gamma_k \equiv \mathrm{Re}(\mu_k)$ and $\omega_k \equiv \mathrm{Im}(\mu_k)$, it is easy to work out that for each pair of complex conjugated eigenvalues, μ_k and μ_{k+1} we will have a pair of real patterns $\mathbf{p}_k = \mathrm{Re}(\mathbf{u}_k)$ and $\mathbf{q}_k = \mathrm{Im}(\mathbf{u}_k)$ associated to a frequency ω_k, a period T_k and a damping factor γ_k. These are the Principal Oscillation Patterns (POP) of the system at that frequency. For each pair of POP derived from a pair of complex eigenvectors, Eq. (9) prescribes the following evolution in time:

$$\mathbf{p}_k \xrightarrow{T_k/4} -\mathbf{q}_k \xrightarrow{T_k/4} -\mathbf{p}_k \xrightarrow{T_k/4} \mathbf{q}_k \tag{10}$$

The evolution in time for each pair can also be obtained empirically from the $\mathbf{z}$ vectors. If we collect the eigenvectors or patterns into a matrix W, with elements ($\mathbf{w}_j = \mathbf{p}_j$, $\mathbf{w}_{j+1} = \mathbf{q}_j$, $j = 2k - 1$, $k = 1, l_i$) and ($\mathbf{w}_j = \mathrm{Re}(\mathbf{u}_k)$, $k = l_i + 1, n$), then $\mathbf{z}_i = W\mathbf{s}_i$ and the time coefficients $\mathbf{s}_i$ can be obtained as

$$\mathbf{s}_i = W^{-1}\mathbf{z}_i \tag{11}$$

References

Alexander MA, Matrosova L, Pendland C, Scott JD, Chang P (2011) Forecasting Pacific SSTs: linear inverse model predictions of the PDO. J Clim 1:385–402

Barston AG, Livezey RE (1987) Classification, seasonality and persistence of low-frequency atmospheric circulation patterns. Mon Weather Rev 115:1083–1126

Brown TJ, Hall BL (1999) The use of t-values in climatological composites analysis. J Clim 12:2941–2944

Conte M, Giuffrida A, Tedesco S (1989) The Mediterranean Oscillation impact on precipitation and hidrology in Italy. Climate water. Publications of the Academy of Finland, Helsinki

Dommenget D, Latif M (2000) Interannual to decadal variability in the tropical Atlantic. J Clim 13:777–792

ElsnerJB Jagger TH (2006) Prediction models for Annual U. S. hurricane counts. J Clim 19:2935–2952

Enfield DB, Mestas-Núñez AM, Mayer DA, Cid-Serrano L (1999) How ubiquitous is the dipole relationship in the Tropical Atlantic sea surface temperatures? J Geophys Res 104:7841–7848

Enfield DB, Mestas-Núñez AM, Trimble PJ (2001) The Atlantic multidecadal oscillation and its relation to rainfall and river flows in the continental U.S. Geophys Res Lett 28:2077–2080

Fisher RA (1921) On the 'probable error' of a coefficient of correlation deduced from a small sample. Metron 1:132

Frankignoul C, Sennechael N (2007) Observed influence of North Pacific SST anomalies in the atmospheric circulation. J Clim 20:592–606

Foltz GR, McPhaden MJ (2008) Trends in Saharan dust and tropical Atlantic climate during 1980–2006. Geophys Res Lett 35: L20706

Gangoiti G, Alonso L, Navazo M, García JA, Millán MM (2006) North African soil dust and European pollution transport to America during the warm season: hidden links shown by a passive tracer simulation. J Geophys Res 111:1–25

Hasselmann K (1988) PIPs and POPs: the reduction of complex dynamical systems using principal interaction and oscillation patterns. J Geophys Res 93:11015–11021

Hoskins BJ, Karoly D (1981) The steady linear response of a spherical atmosphere to thermal and orographic forcing. J Atmos Sci 38:1179–1196

Janowiak JE (1988) An investigation of interannual rainfall variability in Africa. J Clim 1:240–255

Jones PD, Jonsson T, Wheeler D (1997) Extension of the North Atlantic Oscillation using early instrumental pressure observations from Gibraltar and South-West Iceland. Int J Climatol 17:1433–1450

Kallos G, Asthita M, Katsafados P, Spyrou C (2007) Long range transport of anthropogenically and naturally transported particulate matter in the Mediterranean and North Atlantic: current state of knowledge. J Appl Meteorol Climatol 46:1230–1251

Kaylor RE (1977) Filtering and decimation of digital time series. Institute for Physical Science and Technology, Technical report BN850, 144 pp. Available from the Institute of Physical Science and Technology, University of Maryland, College Park

Lamb PJ, Peppler RA (1987) North Atlantic Oscillation: concept and applications. Bull Am Meterorol Soc 68:1218–1225

Landsea CW, Pielke RA Jr, Mestas-Núñez AM, Knaff JA (1999) Atlantic basin hurricanes: indices of climatic change. Clim Change 42:89–129

Lau K, Kim KM (2007) Cooling of the Atlantic by Saharan dust. Geophys Res Lett 34:L23811

Li LZX (2006) Atmospheric GCM response to an idealized anomaly of the Mediterranean Sea surface temperature. Clim Dyn 27:543–552

Lionello, P, Malanotte-Rizzoli, P, Boscolo, R (eds) (2006) Mediterranean climate variability. Elsevier, Amsterdam

Mariotti A, Zeng N, Lau KM (2002) Euro-Mediterranean rainfall and ENSO—a seasonally varying relationship. Geophys Res Lett 29:L014248

Masina S, di Pietro P, Navarra A (2004) Interannual to decadal variability in the North Atlantic from an ocean data assimilation system. Clim Dyn 23:531–546

Millán M (2007) Climate/water cycle feedbacks in the Mediterranean: the role of land-use changes and the propagation of perturbations at the regional and global scale. In: Mellouki A, Ravishankara AR (eds) Regional climate variability and its impacts in the Mediterranean area. Springer, Berlin, pp 83–101

Millán M et al (2005) Climatic feedbacks and desertificaction: the Mediterranean model. J Clim 18:684–701

Mitchel JD, Jones M (2005) An improved method of constructing a database of monthly climate observations and associated high-resolution grids. Int J Climatol 25:693–712. doi:10.1002/joc.1181

Moulin C, Lambert CE, Dulac F, Dayan U (1997) Control of atmospheric export of dust from North Africa by the North Atlantic Oscillation. Nature 387:691–694

Orlanski I, Solman S (2010) The mutual interaction between external Rossby waves and thermal forcing in the subpolar regions. J Atmos Sci 67:2018–2038

Park DB, Latif M (2005) Ocean dynamics and the nature of air sea interactions over the North Atlantic at decadal timescales. J Clim 18:982–995

Penland C, Magorian M (1993) Prediction of Niño 3 sea surface temperature anomalies using linear inverse modeling. J Clim 6:1067–1176

Prospero JM, Lamb PJ (2003) African droughts and dust transport to the Caribbean: climate change indications. Science 302:1024–1027

Prospero J M (2006) Saharan dust impacts and climate change. Oceanography 19:60–61

Rayner NA, Parker DE, Horton EB, Folland CK, Alexander LV, Rodwell DP, Kent EC, Kaplan A (2003) Global analyses of SST, sea ice and night marine air temperature since the late ninteenth century. J Geophys Res 108:4407

SánchezGómez E, Terray L (2005) Large scale atmospheric dynamics and local intense precipitation episodes. Geophys Res Lett 32. doi:10.1029/2005GL023990

Schlesinger ME, Ramankutty K (1994) An oscillation in the global climate system of period 65–70 years. Nature 367:723–726. doi:10.1038/367723ao

Terray P, Delecluse P, Labattu S, Terray L (2003) Sea surface temperature associations with the late Indian summer monsoon. J Clim 21:593–618

Trigo RM, Osborn TJ, Corte-Real JM (2002) The North Atlantic Oscillation influence on Europe: climate impacts and associated physical mechanisms. Clim Res 20:9–17

Tsimplis MN, Alvarez-Fanjul E, Gomis D, Fenoglio-Marc L, Perez B (2005) Mediterranean sea level trends: atmospheric pressure and wind contribution. Geophys Res Lett 32. doi:10.1029/2005GL023867

Trenberth K (1984) Signal versus noise in the Southern Oscillation. Mon Weather Rev 112:326–332

Uppala S et al (2004) ERA-40: ECMWF 45-year reanalysis of the global atmosphere and surface conditions 1957–2002. Newsletter 101, European Center for Medium Range Weather Forecasts, UK

van Oldenborg GJ, Burgers G, Klein Tank A (2002) On the El Niño teleconnections to spring precipitation in Europe. Int J Climatol 20:565–574

von Storch H, Burger G, Schnur R, von Storch JS (1995) Principal oscillation pattern: a review. J Clim 8:377–400

Vorosmarty CJ, Fekete BM, Tucker B A (1998) Global river discharge database (RivDis) V1.1. Available at http://www.daac.ornl.gov

Wu L, Feng H, Zhenyu L (2007) Atmospheric teleconnections of tropical Atlantic variability: interhemispheric, tropical-extratropical and cross basin interactions. J Clim 33:856–870

Zhang R, Delworth TL (2006) Impact of Atlantic multidecadal oscillations on India/Sahel rainfall and Atlantic hurricanes. Geophys Res Lett 33:L17712. doi:10.1029/2006GL026267